Wafer-scale process for fabricating arrays of nanopore devices

Amir G. Ahmadi
Georgia Institute of Technology
School of Chemical and Biomolecular Engineering
311 Ferst Drive
Atlanta, Georgia 30332-0100

Zhengchun Peng
Peter J. Hesketh
Georgia Institute of Technology
Woodruff School of Mechanical Engineering
801 Ferst Drive
Atlanta, Georgia 30332-0405

Sankar Nair
Georgia Institute of Technology
School of Chemical and Biomolecular Engineering
311 Ferst Drive
Atlanta, Georgia 30332-0100
E-mail: sankar.nair@chbe.gatech.edu

Abstract. Nanopore-based single-molecule analysis is a subject of strong scientific and technological interest. Recently, solid state nanopores have been demonstrated to possess advantages over biological (e.g., protein) pores due to the relative ease of tuning the pore dimensions, pore geometry, and surface chemistry. Previously demonstrated methods have been confined to the production of single nanopore devices for fundamental studies. Most of these techniques (e.g., electron microscope beams and focused ion beams) are limited in scalability, automation, and reproducibility. We demostrate a wafer-scale method for reproducibly fabricating large arrays of solid state nanopores. The method couples high-resolution electron-beam lithography and atomic layer deposition (ALD). Arrays of nanopores (825 per wafer) are successfully fabricated across 4-in. wafers with tunable pore sizes. The nanopores are fabricated in 16- to 50-nm thin silicon nitride. ALD of aluminum oxide is used to tune the nanopore size. By careful optimization of the processing steps, a device survival rate of up to 96% is achieved on a wafer with 50-nm thin silicon nitride films. Our results facilitate an important step in the development of large-scale nanopore arrays for practical applications such as biosensing. © *2010 Society of Photo-Optical Instrumentation Engineers.* [DOI: 10.1117/1.3486202]

Subject terms: nanopores; nanopore array; electron-beam lithography; solid state nanopore fabrication; nanotechnology; atomic layer deposition.

Paper 10007R received Feb. 10, 2010; revised manuscript received Jul. 20, 2010; accepted for publication Jul. 26, 2010; published online Sep. 7, 2010.

1 Introduction

Functional nanopores (e.g., those in nanoporous zeolites[1] or nanotubes[2,3]) are already important in many technological areas including energy-efficient separations, energy conversion, and chemical or biomolecule sensing. In these applications, the collective behavior of all the pores in the nanoporous material or thin film is of primary interest. However, nanopores that function as individually addressable devices, or "engineered nanopore devices" (ENDs), have become a subject of growing interest and offer a promising route toward applications such as ultrarapid sensing and analysis of chemical and biological analytes[4] (e.g., small molecules, DNA, proteins). The first ENDs were produced from "soft matter" in the form of channel-forming bacterial proteins such as α-hemolysin (α-HL) reconstituted in synthetic lipid bilayers. The α-HL nanopore has been studied extensively as an ion channel for metering the length and sequence of DNA. As strands of DNA pass through the nanopore, the resulting modulations in the ionic current through the nanopore can be measured and used to characterize the length and composition of the strand. Unfortunately, the complex geometry of the pore limits the device resolution, and thus far, the goal of distinguishing strands that differ by a single nucleotide has not been attained. There are also other intrinsic disadvantages in working with nanopores made from soft matter.[5–7] Biological nanopores are not very robust and cannot be maintained for extended periods. In addition, there are limited options for controlling the pore geometry and dimensions for practical applications. These issues have led to a shift toward fabrication of solid state inorganic nanopores that enable greater robustness and better control over pore geometry.

Nanopores formed in solid state materials are subject to completely different design considerations that resemble those found in semiconductor and microelectronic device manufacturing. Figure 1 shows a design schematic of a solid state END. Two critical design considerations are the pore size and length, which are chosen for the desired application. For example, in DNA sensing, the pore diameter desired is in the range of 2 to 10 nm, whereas larger pores may be suitable for the detection of protein analytes. The free-standing film is generally desired to be as thin as possible (e.g., 10 to 50 nm), while still being mechanically robust and defect-free. The substrate is silicon, whereas sili-

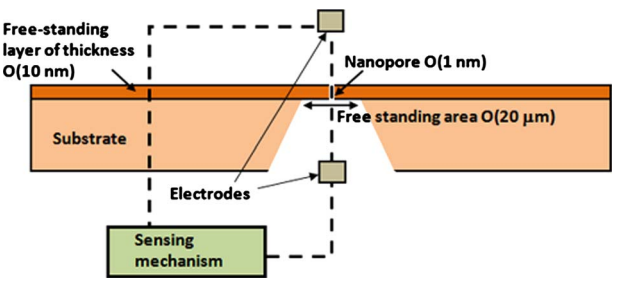

Fig. 1 Solid state END geometry and design considerations.

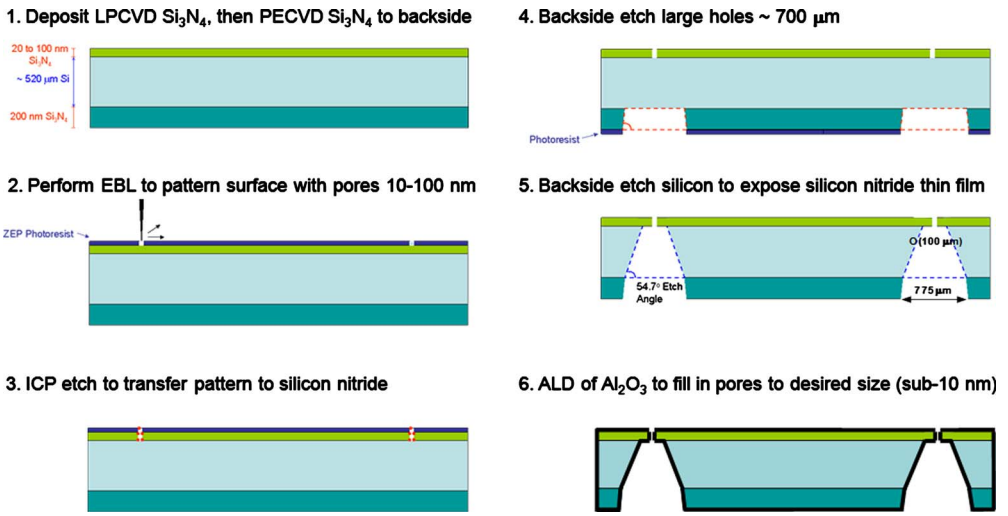

Fig. 2 Major process steps in tunable fabrication of arrays of nanopores on a wafer.

con dioxide (SiO_2) and/or silicon nitride (Si_3N_4) are grown or deposited to form the free-standing film containing the nanopore. The processing strategy starts with fabrication of relatively large holes followed by the reduction of pore size (usually by at least an order of magnitude), until a nanopore of desired size is formed.

A common solid state END fabrication method[8,9] uses a focused ion beam (FIB) to produce nanopores. The incident ions remove surface material on the atomic scale and single nanopores in the sub-10-nm-diameter range have been demonstrated via FIB etching.[10,11] However, efforts to improve reproducibility remain ongoing. This reproducibility of FIB-fabricated sub-20-nm pores is limited by the challenges in maintaining identical process conditions including ion flux, charging effect, and processing temperature at different milling spots. Another issue associated with FIB milling is the lateral deposition of milled material, which increases the surface roughness of the pores around the edges. One variation uses FIB to produce larger pores of 70-nm size and fills them in to achieve 12-nm pores by depositing aluminum nitride.[12] Similar approaches to pore shrinkage have also been reported using electron-beam-induced deposition[13] and hydrocarbon deposition using an electron beam.[14] So far, no FIB-based method has demonstrated arrays of high-quality sub-20-nm pores across an entire wafer. Another method used to produce nanopores involves the application of a tightly focused, high-voltage (200 to 300 keV) electron beam (generated in a transmission electron microscope) to etch a thin free-standing membrane supported on a silicon wafer.[15–21] The film is usually silicon nitride or silicon dioxide (20 to 50 nm thin), deposited and exposed using standard photolithography and etching steps. This method also has drawbacks: it requires a large amount of operator time, cannot be easily automated, and is not scalable.

The objective of this paper is to demonstrate a fully wafer-scalable process for fabricating a large number (e.g., ~1000) of individually addressable nanopore devices on a 4-in. wafer. The nanopores are shown to be tunable in size from 50 to below 20 nm, and are fabricated reproducibly with high throughput. Pores smaller than 20 nm are easily accessible by the present process, but are not reported in this paper since they cannot be easily imaged on the wafer. The thin films containing the pores are very uniform and tunable in thickness from 20 to 50 nm. In this paper, we demonstrate the fabrication of more than 800 devices on a wafer, and a sufficient number of devices are characterized at each step to obtain a reliable statistical estimate of the effectiveness of each step.

2 Methods

Figure 2 illustrates the major steps in the nanopore fabrication process. Most handling and device processing steps were performed in a class 100 clean room (CR) environment, except that the electron-beam lithography (EBL) step is performed in a class 10 CR and the KOH etch in a class 1000 CR. The substrates used were 400- or 520-μm-thick double-side polished ⟨100⟩ oriented silicon wafers. The wafers were immersed in 2% hydrofluoric acid solution to remove any native silicon dioxide immediately prior to processing. Figure 2 illustrates the major fabrication steps in the process. Silicon nitride (Si_3N_4) films in the 15- to 50-nm thickness range were deposited on a wafer using low-pressure chemical vapor deposition (LPCVD) at 800 °C. The precursors were ammonia and dichlorosilane. Film thickness was measured at 9 to 13 points by ellipsometry. Next, EBL was performed using a Zeon ZEP-520 *e*-beam resist. The pattern consisted of a 29×29 array of nanopores spaced 2.47 mm apart, with alignment markings near the edges. Larger features were patterned around 25 of the pores across the wafer, enabling these pores to be easily located in scanning electron microscopy (SEM) analysis. These pores were imaged by SEM to give the size distribution and geometry. The wafer was then etched in an inductively coupled plasma (ICP) to transfer the pattern from the resist to the Si_3N_4. The precursors used were tetrafluoromethane and oxygen. Any remaining resist was removed, and the wafer underwent ellipsometry and SEM imaging to confirm pattern transfer. Next, photolithography with backside alignment was performed to pattern an array of 675×675 or 775×775-μm windows on the backside of the

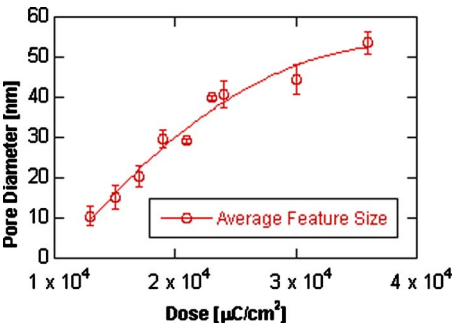

Fig. 3 Average pore size as a function of dose in 100-nm ZEP 2:1 after development. The curves are only a guide to the eye.

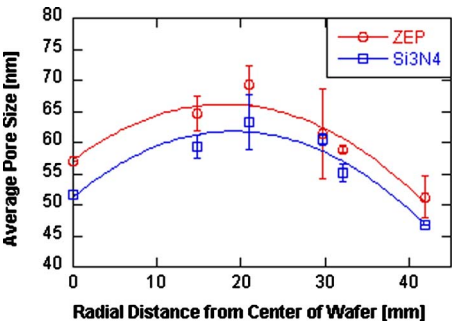

Fig. 5 Patterned nanopore size as a function of radial distance on the wafer before and after pattern transfer. The curves are only a guide to the eye.

wafer. To obtain a high device survivability, the wafers were carefully wet-etched using a specially designed holder, in a 45% KOH (w/w) solution with isopropanol (IPA) at 80 °C or higher to expose the free-standing films and open the other end of the pores. Optical microscopy was used to determine survival rate (yield) and quality of the devices. The open pores were then imaged by SEM. Finally, atomic layer deposition (ALD) of Al_2O_3 was performed to "fill in" the open pores to a smaller size. The precursors used were trimethyl aluminum and water vapor with respective pulse times of 15 and 5 ms, and at a temperature of 255 °C. SEM images were taken between 107 cycles at a time.

3 Results and Discussion

Optimization of multiple steps in the process was found to be critical to obtain a wafer with a high yield of good-quality nanopores. Therefore, a set of important parameters was rigorously monitored between every process step to obtain the first clear results on reproducibility and quality of nanopore fabrication process steps. These parameters include the thickness and uniformity of the film containing the nanopore; the size distribution, geometry, and SEM contrast of the nanopores; and the appearance of the front and backside surfaces, i.e., number of stray deposited particles, scratches, and other defects. Several wafers and individual devices underwent different degrees of processing to demonstrate reproducibility and to show the range of pore sizes and film thicknesses that are possible in the presented process.

The first step investigated was the patterning of the initial array of pores in the electron beam resist via EBL. The pores were patterned using two methods of dosing. In the first, a single shot of the beam was applied with a very high dose. In the second, multiple shots of the beam were applied at significantly lower doses. Comparable nanopore size and quality were achieved with both methods. A single

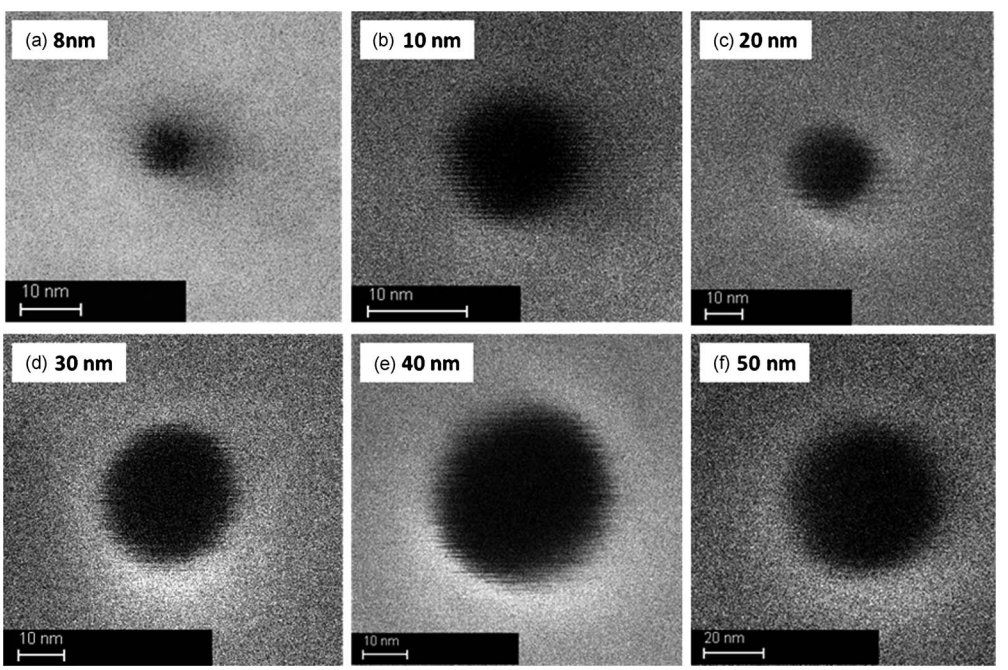

Fig. 4 High-resolution SEM images of nanopores of varying sizes patterned in 100-nm-thick ZEP2:1 resist films at different doses. From (a) to (f), pore sizes of 8, 10, 20, 30, 40, and 50 nm (see Fig. 3 for corresponding electron doses).

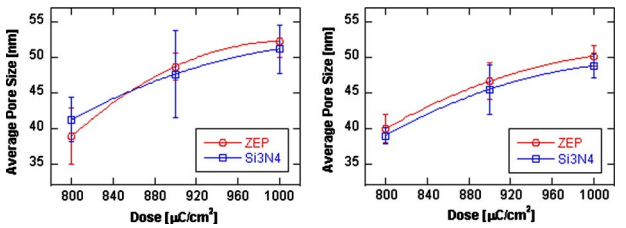

Fig. 6 Pore size as a function of dose for two wafers after identical processing. The curves are only a guide to the eye.

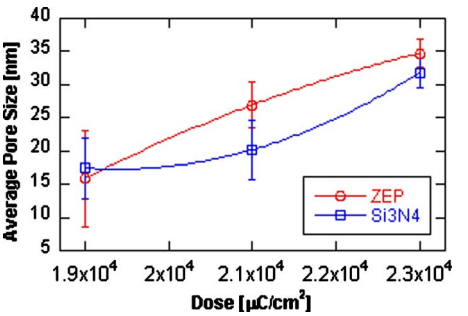

Fig. 7 Pore size as a function of dose before and after pattern transfer for single-shot dosing. The curves are only a guide to the eye.

silicon wafer underwent three trials in which every parameter was kept constant except for the electron dose. The pores were patterned by a single shot of the beam at a current of 2 nA. The resist used was ZEP diluted 2:1 in anisole (ZEP2:1) and coated at 3000 rpm to give a thickness of about 100 nm. In each trial, the array of pores was split into three regions, each of which received a different dose. Fifteen pores were viewed in SEM after patterning (five per dose) to obtain the size distribution. At the end of each trial, the wafer was immersed in a stripping solution for 15 min, and washed with acetone, methanol, and isopropanol before being patterned again. The effects of electron dose on pore size are given in Fig. 3. As clearly demonstrated by the figure, one can precisely pattern the initial pore size in the 10- to 50-nm range by varying the electron dose. The low statistical fluctuation in the patterned pore dimensions (indicated by the error bars in Fig. 3) validates the use of EBL as an excellent first step for nanopore array fabrication. The smallest nanopore produced was 8 nm in diameter. The pores observed in SEM demonstrated high contrast with well-defined edges and circular geometry, even as the pore size was reduced to 10 nm and smaller. Several examples are shown in Fig. 4.

In the next set of experiments, four wafers underwent EBL and pattern transfer to the silicon nitride, followed by resist removal. The process parameters examined include film and resist thickness, dose, shot pitch, and the pore pattern. The pore pattern was a 50-nm circle divided into multiple shots with a shot pitch of 5 nm. Because the pattern was divided into multiple shots, the dose required for each shot was much lower than the pores patterned by a single shot. The first wafer was coated with 22 ± 5-nm silicon nitride, then coated with 130-nm ZEP2:1, and patterned with a constant dose of 500 $\mu C/cm^2$ across the entire array of pores. Nineteen pores were imaged across the wafer after resist development and after pattern transfer to the silicon nitride. The pore size distribution was found to be a function of the radial distance from the center of the wafer, as shown in Fig. 5. This is a controllable phenomenon, which results from the variations in resist thickness during spin coating. It is suggested that the plot in Fig. 5 qualitatively reflects the thickness profile of the spin-coated resist. The degree of variation is significant, and therefore the eventual manufacturing process for nanopores arrays should incorporate a radially varying dose profile in the patterning step, or tuning the spin-coating process to give a more uniform ZEP film. The pore size was also found to shrink by an average of 7% after pattern transfer, which is expected as ICP etch usually leads to a slightly tapered sidewall.

Next, two wafers underwent identical processes to demonstrate reproducibility. Both wafers were coated with 12 ± 4-nm silicon nitride, then coated with 120-nm ZEP2:1, and patterned with 30-nm circles in three dosing regions. The size distributions are given in Fig. 6. The pore sizes produced on each wafer are very similar and follow the same trends as a function of electron dose. The somewhat larger standard deviations are most likely due to the dependence of dose on position (see Fig. 5). For example, the electron dose of 900 $\mu C/cm^2$ was delivered to pores that covered the largest span of radii on the wafer, and therefore would be expected to have the greatest variance in size, and thus the highest standard deviation. These effects appear to average out to give a mostly unbiased electron dose dependence of the patterned pore size.

The fourth wafer was deposited with 19 ± 3-nm silicon

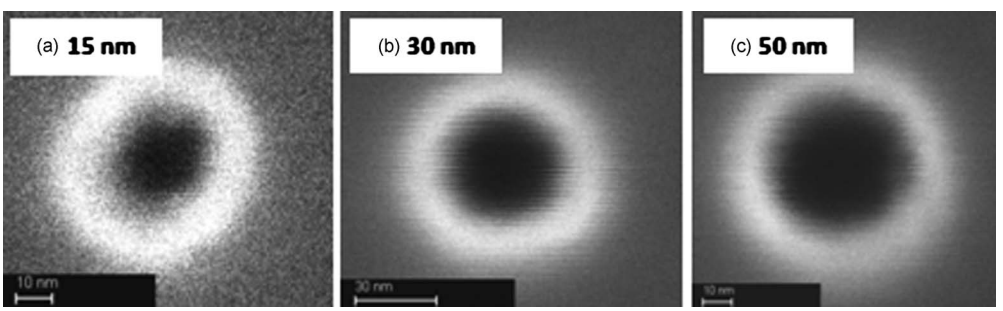

Fig. 8 Nanopores of various diameters transferred from the e-beam resist to the silicon nitride films; (a) and (b) in 16-nm silicon nitride and (c) in 7-nm silicon nitride.

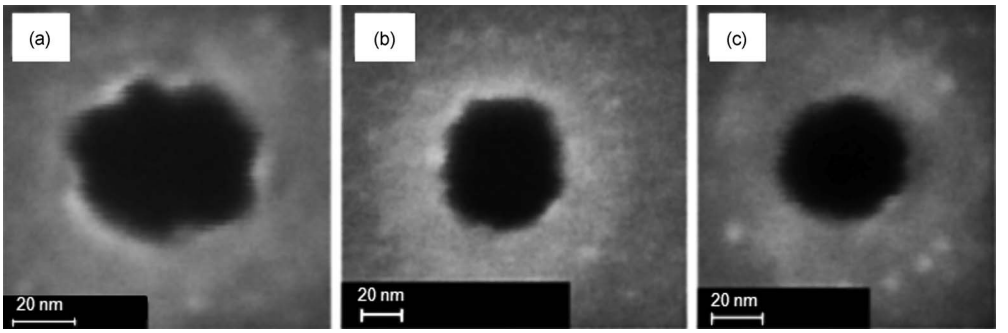

Fig. 9 Three isolated pores unmarked by calibration features showing the types of imperfections that can occur during processing: (a) and (b) jagged pores created by unoptimized doses in 7-nm and 16-nm silicon nitride, and (c) good-quality circular pore created by optimized dose in 7-nm silicon nitride.

nitride and coated with 100-nm ZEP2:1. The pores were patterned using a single shot in three dosing regions. This result is shown in Fig. 7. Again, a highly reproducible and tunable pore size was obtained upon variation of the electron dose.

The smallest pore size produced in silicon nitride was about 15 nm. SEM images of the different size pores are shown in Fig. 8. The pores have high contrast under the imaging electron beam, and demonstrate good transfer of the circular geometry. It was found that EBL patterning using a single shot yields the smallest pores with the best geometrical characteristics.

Outside of our test set of 25 pores marked by the calibration features, a number of the other pores on the wafer (which are not marked by calibration features) were also successfully located for characterization (by trial and error). Three examples of these pores are shown in Fig. 9. There appear to be two kinds of occasional imperfections [Figs. 9(a) and 9(b)] that occur in these isolated features. The first is a wavelike roughness at the edges of the pore. The second is an apparent elongation of the circular shape in the lateral direction, resulting in an elliptical pore. These effects are due to nonideal dosing of the resist during EBL. They do not generally occur in pores surrounded by calibration features because of a proximity effect (these pores receive an added dose that is symmetrical about the pore, resulting in a more circular geometry). To minimize such defects, the dose should be optimized for a given resist thickness. Figure 9(c) shows the result from a properly dosed (800 $\mu C/cm^2$), isolated 50-nm pore.

Tapping-mode atomic-force microscopy (AFM) was performed on a wafer containing 50- to 70-nm pores in a 16 ± 1-nm silicon nitride film. The AFM probe was composed of silicon, and had a tip curvature of ~ 8 nm with a tip cone angle of 30 deg. The 1-D profile of a typical pore is shown in Fig. 10. The depth reached by the tip indicates that not only has the pore been etched to the underlying silicon wafer, but also that it was overetched to a significant depth in the silicon itself. This indicates that the etchant molecules are still able to effectively remove material in these nanoscale trenches, and therefore there is room to produce even smaller pores. The measurement bars are placed at a depth of 16 nm, where they are measured to be 66 nm apart for the example shown in Fig. 10. This strongly supports the SEM data. The tapered shape of the profile near the bottom of the profile is an artifact mirroring the shape and size of the tip of the AFM probe. Still, the smallest lateral distance measured is 6.5 nm, suggesting that the actual profile comes to an even sharper peak in the sub-5-nm range.

ALD (Refs. 22 and 23) of aluminum oxide was then performed on the nanopore arrays. Up to 215 ALD cycles were performed. Figure 11 shows the measured pore size as a function of the number of cycles, for two pores of initial size 38 and 45 nm, respectively. Figure 11 also shows the average pore size reduction of 25 pores on a wafer that underwent ALD. For the two individual pores, the aluminum oxide deposition rate (and hence the rate of pore size shrinkage) is nearly linear, with an average deposition rate of 0.58-Å Al_2O_3 per cycle. The nanopore diameters were

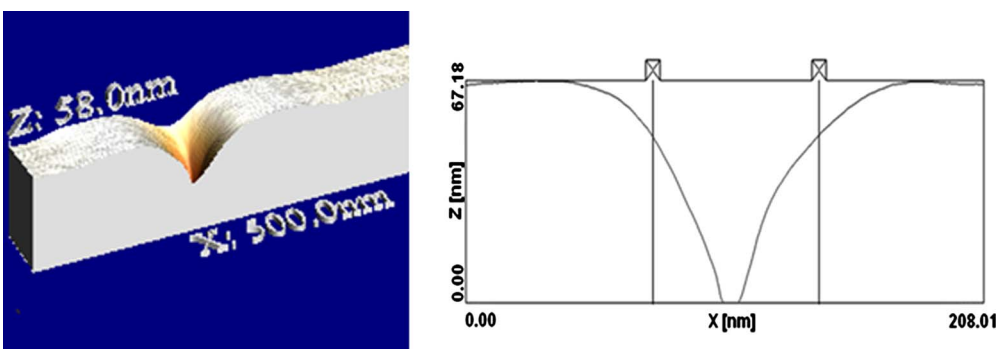

Fig. 10 AFM depth profile (left) and the profile cross section (right) of a 50-nm to 60-nm pore in 16-nm thin silicon nitride film.

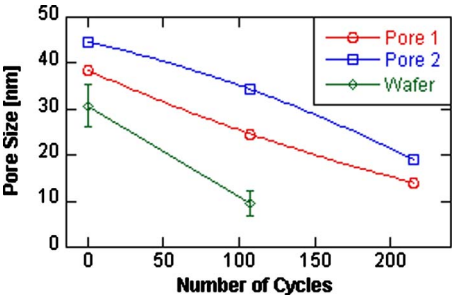

Fig. 11 Nanopore size as a function of number of ALD cycles for two pores (with a deposition rate of 0.58-Å Al_2O_3 per cycle) and an entire wafer (with a deposition rate of 0.9-Å Al_2O_3 per cycle). The curves are only a guide to the eye.

successfully downsized to 20-nm levels. Figure 11 also clearly indicates that the pore size can be easily scaled below 20 nm by additional ALD cycling [as demonstrated by other authors with individual nanopores,[24] and also suggested by Fig. 12(d)]. However, once these pores were sized below 20 nm, their sizes could not be clearly measured by SEM. Figure 12 shows SEM images of pore 2 (from Fig. 11) at different stages of ALD processing. By the last set of cycles, the pore has been very nearly closed. Under the same conditions, a wafer containing 25 pores also underwent ALD for 107 cycles. If the rate of material deposited remains constant, the pore size will shrink faster over time. This effect is observed as the pores in the wafer approach the sub-10-nm range. The average deposition rate observed on the wafer was 0.9-Å Al_2O_3 per cycle.

To demonstrate the final process step and investigate the resulting yield of the devices, several wafers were wet etched from the back to expose the free-standing silicon nitride films, each containing a nanopore. The highest aspect ratio (length:thickness) of a surviving free-standing film achieved was 19,750, which demonstrates the high mechanical strength of the membranes.

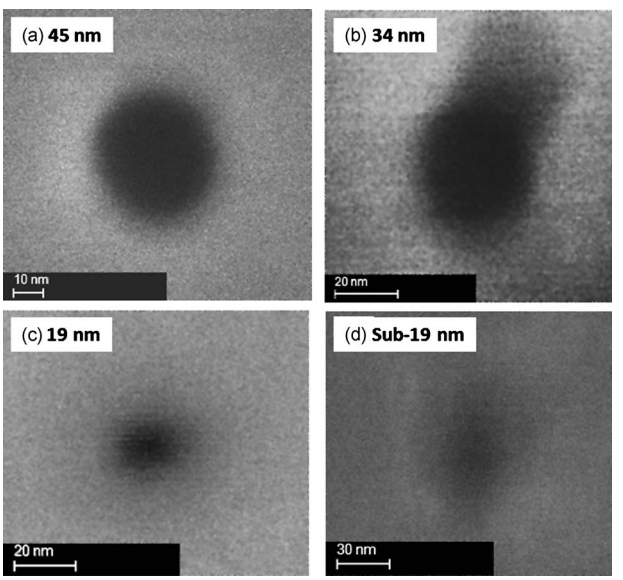

Fig. 12 SEM images of a single nanopore undergoing ALD cycles, as shown in Fig. 11 (pore 2). The nanopore size is reduced in a controlled manner and with nanometer scale precision.

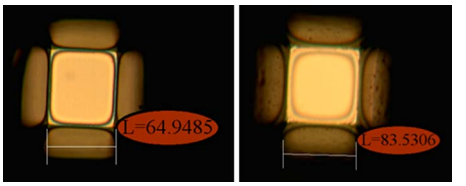

Fig. 13 Optical images of two devices (50-nm silicon nitride) after backside wet etch. The window dimensions shown are in micrometer.

The survival rate of devices following the KOH wet etch was determined by optical microscopy of every device on each wafer. The best results were obtained for wafers containing 50-nm free-standing films with 60- to 80-μm windows. Figure 13 shows examples of these films. A yield of 903 out of 940 devices, or 96% across the wafer, was achieved. Devices at the edges of the wafer were included in the analysis. For the case of the 16 nm films over 200–500 μm windows, the survival rate was 15%. The aspect ratio was likely too large to allow the films to withstand the mechanical stresses arising from the KOH etching process. This result indicates that further optimization of the window dimensions for ultra-thin films is necessary.

4 Conclusions

We have demonstrated a process for fabricating large arrays of nanopores in the sub-20-nm range on a wafer. This is a necessary step toward scaling up the production of nanopore devices. The fabrication process described here has been demonstrated to produce hundreds of devices on a wafer with high throughput, tunable pore size, and reproducibility. In a controlled industrial fabrication environment, this process can be easily scaled up to produce hundreds of thousands of nanopore devices on a single 12-in. wafer. Furthermore, the high precision of the ALD step enables continued pore shrinkage to a few nanometers. The presented process can also be modified for different applications. For example, several pores of different sizes can be patterned on a single device. This may be useful for detecting multiple analytes that vary in size or charge in a solution. If silicon dioxide is deposited instead of aluminum oxide, the pores can thereafter be functionalized for different single-molecule sensing applications.[25,26] ALD of other materials such as titanium oxide[27] or metals[28–30] can also be used to impart different chemical, mechanical, and electrical properties to the nanopores for a desired application.

Acknowledgments

The authors acknowledge financial support from the National Science Foundation (ECCS-#0801829) and Sandia National Laboratories. We acknowledge J. Abdallah, J. Blair, D. Brown, R. Doraiswami, D. Noga, C. Summers, and the staff of the Microelectronics Research Center (Georgia Institute of Technology) for helpful discussions and training on thin-film processing and electron-beam lithography equipment.

References

1. M. E. Davis, "Ordered porous materials for emerging applications," *Nature* **417**(6891), 813–821 (2002).
2. R. H. Baughman, A. A. Zakhidov, and W. A. de Heer, "Carbon nanotubes—the route toward applications," *Science* **297**(5582), 787–792 (2002).
3. J. Goldberger, R. Fan, and P. D. Yang, "Inorganic nanotubes: a novel platform for nanofluidics," *Acc. Chem. Res.* **39**(4), 239–248 (2006).
4. J. J. Kasianowicz, "Nanometer, scale pores: potential applications for analyte detection and DNA characterization," *Dis. Markers* **18**(4), 185–191 (2002).
5. D. W. Deamer and M. Akeson, "Nanopores and nucleic acids: prospects for ultrarapid sequencing," *Trends Biotechnol.* **18**(4), 147–151 (2000).
6. A. Marziali and M. Akeson, "New DNA sequencing methods," *Annu. Rev. Biomed. Eng.* **3**, 195–223 (2001).
7. W. Vercoutere and M. Akeson, "Biosensors for DNA sequence detection," *Curr. Opin. Chem. Biol.* **6**(6), 816–822 (2002).
8. J. Li, D. Stein, C. McMullan, D. Branton, M. J. Aziz, and J. A. Golovchenko, "Ion-beam sculpting at nanometre length scales," *Nature* **412**(6843), 166–169 (2001).
9. J. L. Li, M. Gershow, D. Stein, E. Brandin, and J. A. Golovchenko, "DNA molecules and configurations in a solid-state nanopore microscope," *Nature Mater.* **2**(9), 611–615 (2003).
10. J. Gierak, E. Bourhis, G. Faini, G. Patriarche, A. Madouri, R. Jede, L. Bruchaus, S. Bauerdick, B. Schiedt, A. L. Biance, and L. Auvray, "Exploration of the ultimate patterning potential achievable with focused ion beams," *Ultramicroscopy* **109**(5), 457–462 (2009).
11. N. A. Patterson, D. P. Adams, V. C. Hodges, M. J. Vasile, J. R. Michael, and P. G. Kotula, "Controlled fabrication of nanopores using a direct focused ion beam approach with back face particle detection," *Nanotechnology* **19**(23), 235304 (2008).
12. S. Yue and C. Gu, "Nanopores fabricated by focused ion beam milling technology," in *Proc. 7th IEEE Int. Conf. on Nanotechnology—IEEE-NANO 2007*, pp. 628–631 (2007).
13. R. Kox, C. Chen, G. Maes, L. Lagae, and G. Borghs, "Shrinking solid-state nanopores using electron-beam-induced deposition," *Nanotechnology* **20**(11), 115302 (2009).
14. A. Radenovic, E. Trepagnier, R. Csencsits, K. Downing, and J. Liphardt, "Fabrication of 10 nm diameter hydrocarbon nanopores," *Appl. Phys. Lett.* **93**(18), 183101 (2008).
15. J. B. Heng, A. Aksimentiev, C. Ho, P. Marks, Y. V. Grinkova, S. Sliger, K. Schulten, and G. Timp, "Stretching DNA using an artificial nanopore," *Biophys. J.* **88**(1), 659A–659A (2005).
16. J. B. Heng, A. Aksimentiev, C. Ho, V. Dimitrov, T. W. Sorsch, J. F. Miner, W. M. Mansfield, K. Schulten, and G. Timp, "Beyond the gene chip," *Bell Labs Tech. J.* **10**(3), 5–22 (2005).
17. J. B. Heng, C. Ho, T. Kim, R. Timp, A. Aksimentiev, Y. V. Grinkova, S. Sligar, K. Schulten, and G. Timp, "Sizing DNA using a nanometer-diameter pore," *Biophys. J.* **87**(4), 2905–2911 (2004).
18. U. F. Keyser, B. N. Koeleman, S. Van Dorp, D. Krapf, R. M. M. Smeets, S. G. Lemay, N. H. Dekker, and C. Dekker, "Direct force measurements on DNA in a solid-state nanopore," *Nat. Phys.* **2**(7), 473–477 (2006).
19. D. Krapf, M. Y. Wu, R. M. M. Smeets, H. W. Zandbergen, C. Dekker, and S. G. Lemay, "Fabrication and characterization of nanopore-based electrodes with radii down to 2 nm," *Nano Lett.* **6**(1), 105–109 (2006).
20. A. Mara and Z. Siwy, "An asymetric nanopore for biomolecular sensing," *Biophys. J.* **86**(1), 603A–603A (2004).
21. H. Yan and B. Q. Xu, "Towards rapid DNA sequencing: detecting single-stranded DNA with a solid-state nanopore," *Small* **2**(3), 310–312 (2006).
22. S. J. Yun, K. H. Lee, J. Skarp, H. R. Kim, and K. S. Nam, *Characterization of* Al_2O_3 *Films Grown by Atomic Layer Deposition Using* $Al(CH_3)_3$ *and* H_2O, MRS, San Francisco (1997).
23. S. Jakschik, U. Schroeder, T. Hecht, D. Krueger, G. Dollinger, A. Bergmaier, C. Luhmann, and J. W. Bartha, "Physical characterization of thin ALD-Al_2O_3 films," *Appl. Surf. Sci.* **211**(1–4), 352–359 (2003).
24. P. Chen, T. Mitsui, D. B. Farmer, J. Golovchenko, R. G. Gordon, and D. Branton, "Atomic layer deposition to fine-tune the surface properties and diameters of fabricated nanopores," *Nano Lett.* **4**(7), 1333–1337 (2004).
25. J. Lund, R. Mehta, and B. A. Parviz, "Label-free direct electronic detection of biomolecules with amorphous silicon nanostructures," *Nanomed. Nanotechnol. Biol. Med.* **2**(4), 230–238 (2006).
26. J. Tan, H.-F. Wang, and X.-P. Yan, "Discrimination of saccharides with a fluorescent molecular imprinting sensor array based on phenylboronic acid functionalized mesoporous silica," *Anal. Chem.* **81**(13), 5273–5280 (2009).
27. I. Jogi, M. Pars, J. Aarik, A. Aidla, M. Laan, J. Sundqvist, L. Oberbeck, J. Heitmann, and K. Kaupo, "Conformity and structure of titanium oxide films grown by atomic layer deposition on silicon substrates," *Thin Solid Films* **516**(15), 4855–4862 (2008).
28. L. Zhengwen, A. Rahtu, and R. G. Gordon, "Atomic layer deposition of ultrathin copper metal films from a liquid Copper(I) amidinate precursor," *J. Electrochem. Soc.* **153**(11), 787–794 (2006).
29. H. Kim, "The application of atomic layer deposition for metallization of 65 nm and beyond," *Surf. Coat. Technol.* **200**(10), 3104–3111 (2006).
30. G. A. T. Eyck, J. J. Senkevich, F. Tang, D. Liu, S. Pimanpang, T. Karaback, G. C. Wang, T. M. Lu, C. Jezewski, and W. A. Lanford, "Plasma-assisted atomic layer deposition of palladium," *Chem. Vap. Deposition* **11**(1), 60–66 (2005).

Amir G. Ahmadi received his BTech degree in chemical engineering from Clarkson University, Potsdam, New York, in 2005. He is currently pursuing his PhD degree in chemical and biomolecular engineering at the Georgia Institute of Technology, Atlanta. His research interests are micro/nanofabrication and characterization of functional thin films. He has published a book chapter and given two conference presentations.

Zhengchun Peng received his BS degrees in automotive engineering and in international business from Beijing Institute of Technology, China, in 1998, and his MS degree in mechanical engineering from Louisiana State University, Baton Rouge, in 2003. He was a research associate with the synchrotron radiation Center for Advanced Microstructures and Devices, Baton Rouge, Louisiana. He is currently pursuing his PhD degree in mechanical engineering at the Georgia Institute of Technology, Atlanta. His research interests are micro/nano electromechanical systems and micro/nanofluidics. He has published 10 peer-reviewed journal papers and has given more than 10 conference and invited presentations.

Peter J. Hesketh received his BSc degree in electrical and electronic engineering from the University of Leeds, in 1979 and his MS degree in 1983 and his PhD degree in 1987 in electrical engineering from the University of Pennsylvania. He was with the Microsensor Group at the Physical Electronics Laboratory of Stanford Research Institute and then Teknekron Sensor Development Corporation before joining the faculty in the Department of Electrical Engineering and Computer Science, the University of Illinois, in 1990. He was codirector of the Microfabrication Applications Laboratory from 1995 to 1998 and directed the Microfluidics Center from 1996 to 1998. He is currently a professor of mechanical engineering at Georgia Institute of Technology, a member of the Parker H. Petit Institute for Bioengineering and Biosciences, and director of the MEMS (microelectromechanical systems) Group in the School of Mechanical Engineering. He is past chair of the Sensor Division of the Electrochemical Society and serves on the Ways and Means Committee at ECS. His research interests include microfabrication of chemical and biosensors, in particular microcantilever sensors, microvalves, miniature gas chromatography systems, and the use of stereolithography for microsystem packaging. He has published over 65 journal papers and edited 15 books on microsystems. He is a fellow of the AAAS, ASME, and ECS and a member of ASEE, AVS, and IEEE.

Sankar Nair received his BTech degree in chemical engineering from the Indian Institute of Technology, Delhi, in 1997 and his MS and PhD degrees in physics and chemical engineering, respectively, from the University of Massachusetts, Amherst, in 2002. He was a postdoctoral fellow in the Materials Science and Engineering Laboratory of the National Institute of Standards and Technology, Gaithersburg, Maryland Since 2003, he has been with the School of Chemical & Biomolecular Engineering, Georgia Institute of Technology, Atlanta, where he is currently an associate professor. His research program is directed toward the engineering and understanding of functional porous materials, thin films, and membranes obtained through nanoscale processing strategies. He has published 40 peer-reviewed journal papers, two book chapters, and four patents (granted and pending) and has given more than 50 conference presentations and invited seminars to academia and national laboratories. He received the NSF CAREER Award in 2009. He is a member of AIChE and ACS.